Available online at www.sciencedirect.com

SciVerse ScienceDirect

Physics Procedia 41 (2013) 858 – 869

Physics Procedia

Lasers in Manufacturing Conference 2013

Fundamentals of Energy Conversion and Dissipation in Powder Layers during Laser Micro Sintering

A. Streek*, P. Regenfuss, H. Exner

University of Applied Sciences Mittweida, Technikumplatz 17, 09648 Mittweida, Germany

Abstract

Under consideration of already published approaches, energy absorption and conversion of a laser beam penetrating into a powder layer is described as a function of grain size, grain density, laser beam intensity, and material properties. The simulations are based on a ray tracing algorithm and show typical results of the early dissipation phase regarding the energy form and the spatial distribution in the irradiated powder. An approach for the estimation of the powder layer thickness is proposed; optimum thicknesses are derived. The findings are applied to interpret observations that have been made during laser micro sintering of molybdenum powder.

Keywords: laser; sintering; powder, energy; dissipation; rapid prototyping; additive manufactoring;

1. Introduction

There is a general trend towards further miniaturization despite simultaneously increasing complexity for functional machinery units in the millimeter range with structural resolutions of several micrometer in several fields of application, like implants in prosthetic medicine, Gittard and Narayan, 2010, electronic circuits, respectively supports, Dobrzanski et al., 2010 of the latter. This trend simultaneously requires fabrication technologies, among others also generative freeform technologies with sufficiently high resolutions.

* Corresponding author. Tel.: +49 3727 976313
E-mail address: streek@htwm.de

doi:10.1016/j.phpro.2013.03.159

As an approach to meet this demand research efforts were started in 2001 at Laserinstitut of Hochschule Mittweida to modify and optimize the already established technology of selective laser sintering with the goal to achieve the required resolution.

Very soon it had become evident that mere downscaling of the conventional technology regarding powder size and focus diameter was inadequate to solve the problem. Therefore a novel regime - laser micro sintering - was developed. The amount of attention that was attracted by the first results was followed by various ambitious requests and a high pressure of success. Therefore, the searches for the respective individual solutions had a mainly heuristic character. Because of this, a quantitative description of laser micro sintering that allows for anticipation of the process deviation when material properties, the coating regime and the sinter parameters are changed, has remained an intriguing challenge.

2. State of the art

Tolochko et al., 2000 reported absorption degrees of powders from measurements in an integration sphere. For refractory metals like molybdenum and tungsten the author resumes a 1.5- to 2-fold higher absorption of the powder compared to the solid body, which is generally in accordance with the circumstance that, by backscattering from a powder surface, radiation is more attenuated than by reflection from a macroscopic surface. However, as no information is given regarding the dependence on layer thickness, packing density, particle shape, and particle size distribution, the results are not suitable for general application.

Fischer et al., 2002 presented a calculation that presumed directional isotropy of the radiation in a powder packing already after minor penetration lengths.

Wang and Kruth, 2000 reported an algorithm by which the course and the attenuation of ideal rays are traced, that are repeatedly reflected in a non-diffuse way while penetrating into a random arrangement of spherical particles. The absorbed relative laser power can be calculated as a function of packing density and penetration depth for blends from two mono-disperse powders. Results are shown for three different powder combinations.

An analytical formulation of intrinsic radiation absorption by powders has been published by Gurasov and Kruth, 2005. The results of the proposed model that is based on evenly distributed scattering centers, is in accordance with the cited ray tracing model of Wang and Kruth, 2000.

3. Laser micro sintering and energy dissipation

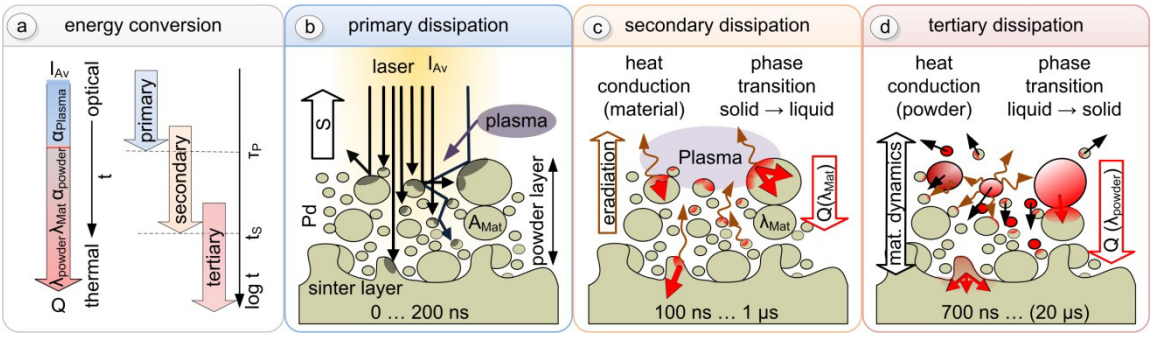

Fig. 1. (a): Three phases of energy dissipation that can be regarded temporally successive if the irradiation period is sufficiently short: Primary dissipation (b): the beam is deflected and absorbed by the powder particles and the substrate; scattering (denoted with the symbol S) is made up by radiation that eradiates from either the upper or lower surface of the layer and cannot be absorbed any more. Secondary dissipation (c): heat conduction occurs over the range of the particles size resulting in heat equilibration inside the particles; heat radiation takes place; liquid and gaseous phases as well as plasma appear including the concomitant dynamic effects. Tertiary dissipation (d): Long range heat conduction into the substrate and inter-particulate heat conduction takes place as well as energy loss through heat radiation and plasma. Liquid material solidifies.

For the purpose of a quantitative approach, the conversion of the laser radiation energy absorbed by the powder packing is considered as a multi-mechanistic process with individual dependencies and influence values. As individual mechanisms “primary”, “secondary”, and “tertiary dissipation” as well as the generation of plasma with the concomitant optical and thermodynamic effects (figure 1 b,c,d) shall be regarded. Laser micro sintering implies irradiation with pulses on a 100 nanosecond time-scale. Although during this irradiation period secondary dissipation will overlap to a limited degree primary dissipation, the mechanisms will be considered as occurring temporally separated, which is equivalent to the assumption of three successive dissipation phases.

During the first one, the primary dissipation phase, high intensity radiation directed toward the surface of the powder packing is scattered and simultaneously (Wang and Kruth, 2000) resulting in a three dimensional distribution of absorbed energy per pulse. This dissipation corresponds to a continuous decrease of radiation intensity along with increasing depth of the respective powder packing horizon. By integration of the change of intensity over the depth and the time a pattern of “primary energy dissipation” in the powder packing can be derived. Influential factors are the optical density of the powder and the material specific degrees of scattering and of absorption (Gurasov and Kruth, 2005).

As mentioned above, especially in the case of long pulse widths, the secondary dissipation phase overlaps partially with the primary one. In this second step the energy dissipates from the outer shell throughout the entire particle. The progression of it depends on thermodynamic material properties and behavior. Next to the coefficient of heat conductivity and the heat capacity it is also the particle size that determines the rate of heat equilibration in a particle and the final temperature of it (Konrad, 2007). Depending on the reach of the intensity after primary dissipation, secondary dissipation into the bulk of the underlying solid (i.e. the substrate or the already sintered body) might have to be regarded.

During, or at the end of this phase, powder particles and the substrate material in contact should have reached such a state of fusion that is prerequisite for the formation of a conjoint melt phase. This transitory

melt phase is crucial for the solidification of the processed powder packing volume and the integration of new material into the sintered specimen.

In the phase of tertiary dissipation, the energy is spreading further throughout the powder packing due to such phenomena that depend on the morphology of the powder, as effective heat conduction in powders, heat radiation, and possibly through convection. Similar to the previous phases, at long pulse widths the slight overlap of the third phase with the second one becomes more pronounced and measurable with increasing pulse width. If no dynamic influences have changed the geometry of the site, the stage of tertiary dissipation at the impact of the following pulse will yield the starting conditions for the next dissipation cycle. In the calculations or simulations of heat conduction the latent heats for phase transitions have to be respected as heat conduction can be noticeably affected.

Plasma can occur during all dissipation phases, provided the thermal energy of a material entity suffices for the temperature raise to boiling point but also for the evaporation enthalpy. Additionally the intensity of the radiation has to exceed a certain threshold value. Plasma effects are: direct attenuation of the incident radiation, delocalization or deformation of solid and fused powder material, and suppression of reactions between the heated material and the environment.

Despite the high importance of the secondary and tertiary dissipation for the performance of laser micro sintering during fabrication, the onset of the sintering process is essentially determined by the initial distribution of thermal energy in the involved materials. Accordingly, the presented article will concentrate on the primary dissipation phase.

4. 3D-powder model and ray tracing

Although the algorithm and the parameters cannot be extracted from the literature and the information is not immediately applicable on any given laser sintering process, the ray tracing model can serve as a useful element in the development of a quantitative description for laser micro sintering. According to the approach of Wang and Kruth, 2000 the incident beam is split into a set of parallel rays; the number of reflections and the lateral position allows for the calculation of the intensity distribution at any level of the powder layer. The model of a stochastically positioned powder layer, with defined size distribution and relative packing density, is generated by a recursive algorithm. The algorithm is based on the presuppositions that the powder particles have an ideally spherical shape and that the material specific absorption degree (ratio of absorbed over incident power) is independent of any other parameters. The number of partial rays can be chosen arbitrarily. Ray tracing is achieved by repeated shift of the virtual powder layer and rotation about the reflection site of the ray on the surface of the particular particle. Simultaneous with the rotation the corresponding attenuation of the ray, which is equivalent to the energy transfer into the respective powder particle, is taken into account. After leaving the virtual powder layer, the calculation of the ray trace is terminated. At this point the powder layer is reoriented into the starting position for the tracing of the next ray.

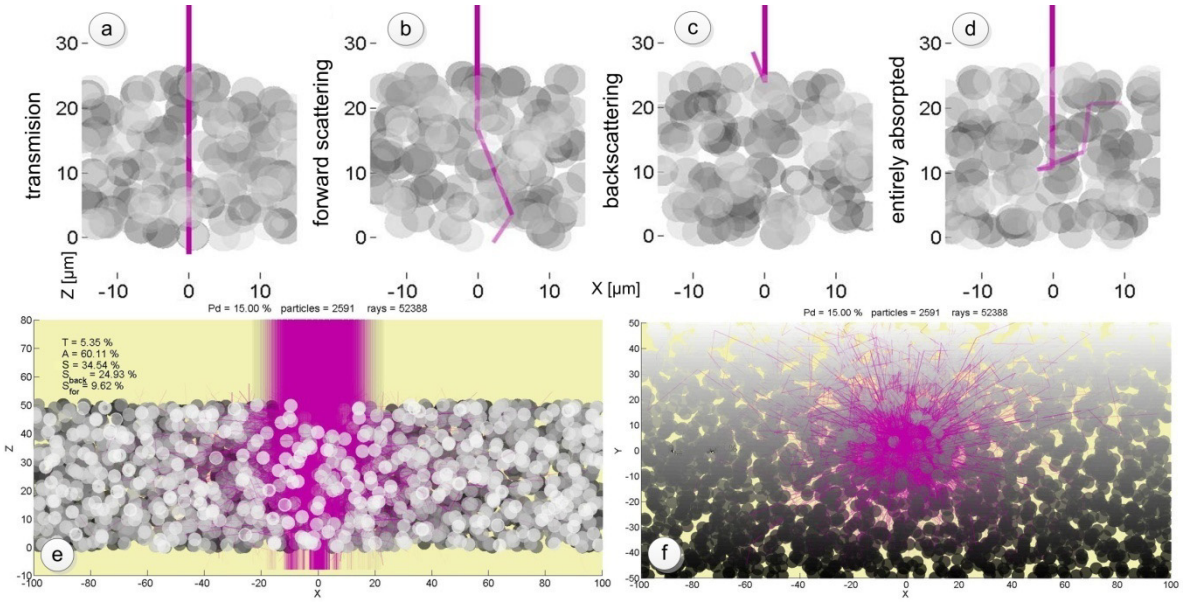

Fig. 2. (a-d): Exemplary fractional rays of a laser beam inciding into the surface of a mono-disperse powder layer (presented as semi-transparent spheres) with a relative packing density of Pd = 15 % and a material specific absorption degree A_{Mat} of 30 % with four different typical scattering traces. a: transmission without deflection; b: forward scattering; c: singular reflection on the surface; d: multiply deflected and attenuated ray. (e-f): Scattering and absorption of a laser beam penetrating through a volume of mono-disperse 5 µm-powder with an absorption degree A_{Mat} = 30 %: Side view (projection) of the powder cuboid and the beam as a bundle of 52,000 fractional rays (e), bottom view onto the same powder layer and the partially scattered and transmitted beam (f). The powder cuboid is composed of ~ 2,600 particles. For the calculation the laser beam is split into ~ 52,000 fractional rays. The simulated dissipation results are: Transmission degree T = 5.35 %, absorption degree of the specific powder layer A = 60 %, overall degree of scattering S = 34.5 %; S is the sum of the amounts of forward scattering S_{for} = 9.6 % and backward scattering S_{back} = 24.9 %.

In figure 2 views of sample rays (fig. 2, a-d) and cross section views (fig. 2, e-f) of the complete bundle are presented respectively. For several sets of powder parameters the components of the beam power that remain as the result of primary dissipation, are calculated as the sum of the individual effects from each of the partial rays. In the case of the chosen material and powder layer a notable amount of radiation (~ 35 %) escapes from the powder layer as reflected radiation, the backward scattering with a ~ 70 % fraction of the overall scattering making up for the largest part. The overall absorption of A_{powder} = 60 % is already twice as high as the absorption A_{mat} = 30 % resulting from a singular reflection from a macroscopic surface of the bulk material. Despite the relatively large thickness, a noticeable, though small, transmission degree T = 5.35 %, meaning the amount of rays that pass the layer without deflection, results.

The larger the number of fractional rays the more realistically the algorithm should resemble the absorption and scattering situation in a powder layer. Phenomena that are not taken account of by this algorithm are the wave character of radiation with the effects of diffraction and interference.

Figure 3 shows the plots versus the vertical position within the powder layer as well as the corresponding 6th degree polynomial fits.

5. Dissipation and power balance of the penetrating beam

The results of the primary dissipation can best be described by comparing the forms into which the originally mono-directional and coherent laser beam power is converted with increasing thickness of a given powder layer. The following are assumed to be characteristic and sufficient to describe the power or energy balances after dissipation of the beam by the respective irradiated powder layer: overall scattering S, absorption A, transmission T, and the amounts of backward and forward scattering S_{back} and S_{for}.

In figure 3, these characteristic amounts are presented in the form of calculated and fitted plots versus powder layer thickness. The values can be likewise considered as the ratios of power over the beam power or the energy over the pulse energy.

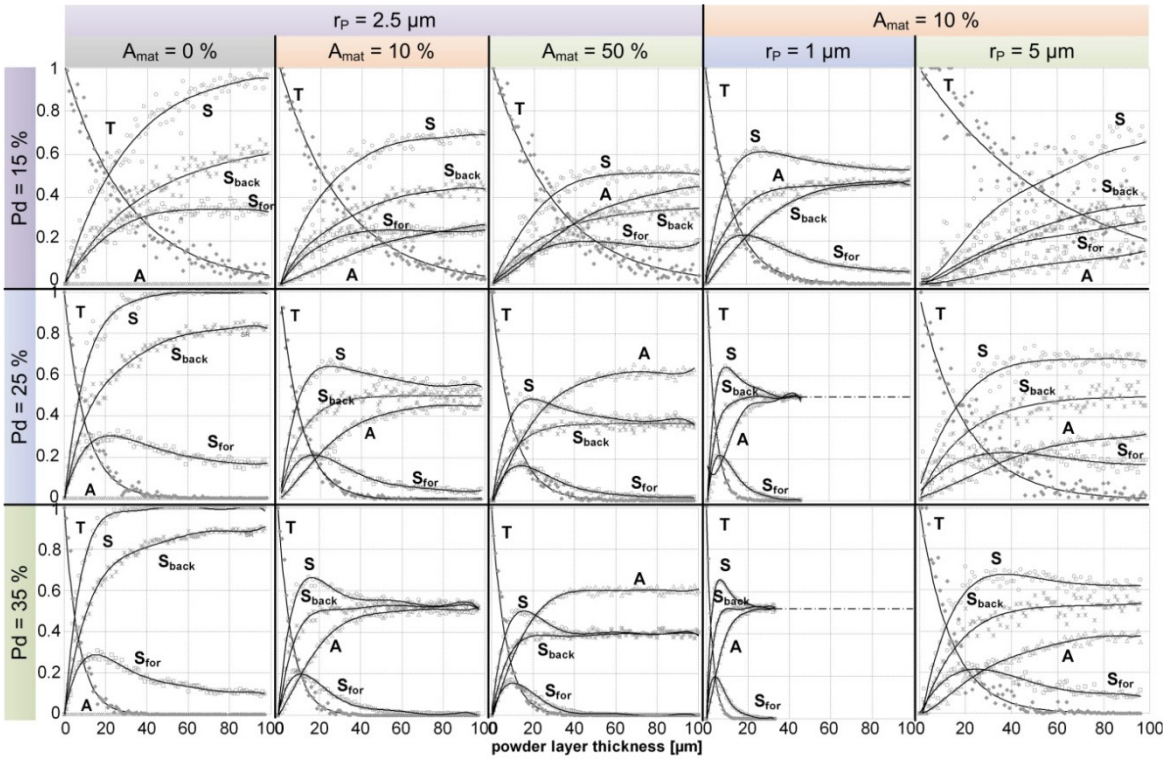

Fig. 3. Simulated relative amounts of the beam power for: S – overall scattering, A - absorption, T - transmission and the amounts of backward and forward scattering S_{back} and S_{for} inside a 5 µm mono-disperse powder layer with thicknesses up to 100 µm. Within the rows the packing densities Pd (10 %, 25 %, and 35 %) are kept constant. For each packing density diagrams are shown for a powder with an absorption degree A_{mat} of 10 % and three different particle radii r_p (1 µm, 1.5 µm, and 5 µm) and for three powders with a particle radius of 2.5 µm and three different material specific absorption degrees A_{mat} (0 %, 10 % and 20 %).

As the influenced powder particles, because of their limited number, do not constitute a statistically relevant ensemble, deviation of the individual simulated values from the fitted curve can be observed. From the diagrams in figure 3 it becomes evident that this deviation from the fitting polynomial decreases with increasing packing density. Transmission merely depends on the packing density, the mean grain size, and the thickness of the powder layer. The combination of these three parameters suffices to determine the optical density (extinction) of the corresponding stochastic arrangement of particles. The calculated curve of the transmitted intensity was not obtained via numerical fitting. It is actually a plot of equation (1) into which the

respective values of particle radius r_P and packing density Pd have been inserted. Equation (1) evolved from a series expansion of the extinction. The extinction has been calculated as the shadowing of a beam passing through a multitude of layers that are incompletely filled with mono-disperse spherical particles.

$$T(z) = e^{\ln\left(1-\frac{3}{2}\cdot Pd\right)\cdot\frac{z}{2\cdot r_P}} \tag{1}$$

In the case of a negligibly small absorption degree $A_{mat} \rightarrow 0$ the curve of the overall scattering $S(z)$ that is composed of $S_{for}(z)$ and $S_{back}(z)$ can be obtained by geometric reflection ("flipping") of the transmission curve across a horizontal line with the ordinate value of 0.5 and vice versa (Fig. 3, left column). Both curves are strictly monotonous. This changes when the material specific absorption degree A_{Mat} becomes greater than zero: Though there is an initial increase of scattering S with increasing depth of the powder layer, the inclination decreases from the very beginning. After passing a maximum it approaches asymptotically a finite limit. This value is also the limit for backscattering $S_{back}(z)$. It is evident that the decline of overall scattering S with increasing depths is due to attenuation of forward scattering S_{for} according to $S(z) = S_{back}(z) + S_{for}(z)$.

The maximum amount of forward scattering $max(S_{for})$ decreases at increasing powder density and at increasing absorption degree of the material and it simultaneously shifts towards thinner powder layers. The subsequent decline of forward scattering S_{for}, which equals the decline in overall scattered radiation S, accounts for the increase in overall absorption A. When the layer has the thickness that is correlate of maximum forward scattering $max(S_{for})$ there is equivalence between transmission and absorption A in the powder layer. At closer investigation of the dependencies it becomes evident that the progression of $A(z)$ has a point of inflection in the same range of thickness z, or in symbolic terms: $z(d^2A/dz^2=0) \approx z(dS_{for}/dz=0)$. After a defined powder layer depth only insignificant change of absorption and scattering will occur along with deeper penetration into any thicker layer. In range of depth transmission is close to zero; therefore the limits for absorption and reflection can be written as $1 = S(z) + A(z)$ for $z \rightarrow \infty$. Logically the limits for $S_{(\infty)}$ and $A_{(\infty)}$ depend merely on the material specific absorption degree.

From the above plots the following empiric relation between the material specific absorption degree (for a single reflection) and the limit for the finally accumulated absorption in an infinitely deep powder layer can be derived:

$$\lim_{z\rightarrow\infty} A_{powder} \approx \sqrt[3]{A_{mat}} \tag{2}$$

This empiric relation has not yet been corroborated by analytical explication. Likewise, the dependence of the absorption $A(z)$, corresponding to $1\text{-}T(z)$ (see equation (1)), upon the material specific absorption A_{mat}, could only be deducted empirically (equation (3)). Nevertheless, it reproduces the results in good approximation.

$$A(z) \approx \sqrt[3]{A_{mat}} \cdot \left(1 - e^{\ln\left(1-\frac{3}{2}Pd\right)\cdot\sqrt[3]{A_{mat}}\cdot\frac{z_{opt}}{2r_P}}\right) \tag{3}$$

The plot of the differential absorption per depth, dA/dz that was calculated numerically by Wang and Kruth, 2000 should be in terms of equation (3) the first derivative. The maximum of the curves dA/dz versus z presented in this work should coincide with the maximum of the forward scattering S_{for} in figure 3. Evidently, this point of inflection is not supported by equation (3).

6. Spatial distribution of the absorbed power from a beam with Gaussian intensity profile

Figure 4 visualizes the spatial distribution of the absorbed portion of a Gaussian shaped laser beam (w_0 = 12.5 µm) penetrating through powder layers. The simulated powder probes vary regarding the types of packing *(Pd* = 15 %; r_p = 2.5 µm; z = 50 µm and Pd = 35 %; r_p = 2.5 µm; z = 25 µm) as well as regarding the powder material specific absorption degrees (A_{mat} = 10 %, 30 %, and 50 %).

From the color marking of the particles it is possible to anticipate the extent and the position of melt phases that could possibly be generated with sufficient energy. From the extent of the ensembles of the noticeably influenced particles (charged with an absorbed power partition above 0.05 %) it can be concluded that the spatial concentration of the absorbed power is higher with high packing densities and high absorption degrees. The shape of the ensembles of these "sinter relevant" particles resembles a flat cylinder with an adjacent upside-down cone underneath, suggesting a restricted volume on top where the fusion of melt phases will be most probable (the "cylinder") and a section below (the "cone") where sintering will be less favored. The red lines mark the horizon the transition from the cylindrically shaped "sinter relevant" section to the cone shaped extension.

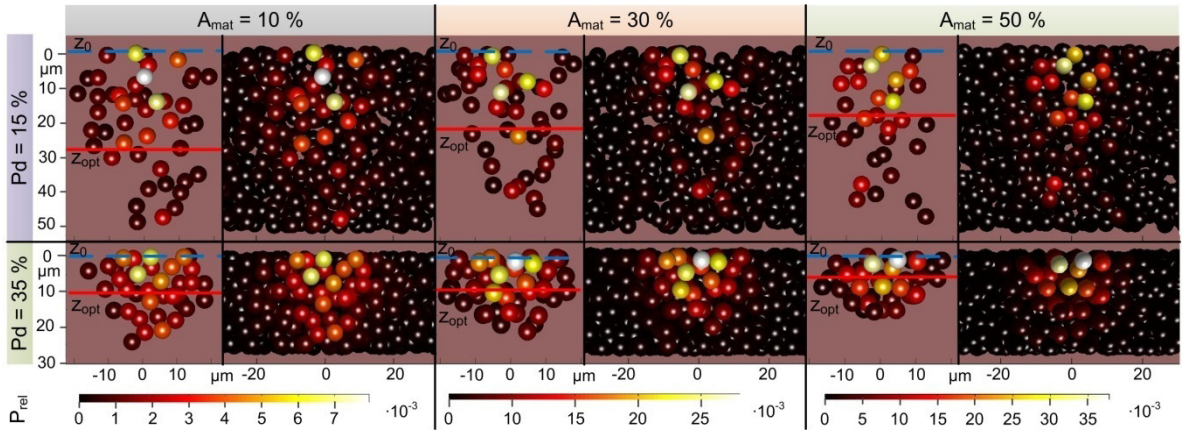

Fig. 4. Simulated cross section views of six powder layers irradiated by a laser beam with a Gaussian intensity profile, a peak intensity I_0 = 1 (arbitrary units), and a waist w_0 = 12.5 µm. The powder layers consist of one of three materials (columns) with the respective material specific absorption degrees A_{mat} 10 %, 30 %, and 50 %. A mono-disperse 2.5 µm particle radius is assumed for all three powders. Of each material two types of powder packings (rows) with the parameters Pd = 15 %, z = 50 µm, r_p = 2.5 µm and Pd = 35 %, z = 25 µm, r_p = 2.5 µm) are simulated. The scale on the right contains the material specific color codings for the absorbed power portions. In the left half of each column the ensembles of the noticeably influenced particles (charged with an absorbed power partition above 0.05 %) are displayed.

7. Estimation of suitable powder layer thicknesses as a function of powder parameters

In order to generate a sinter layer that is sufficiently interconnect with the bulk body underneath, the interface between the fused powder material and the substrate has to consist of sufficient melt from both components of the junction. As can be seen in figure 4 the density of the absorbed power along the beam axis declines rapidly after a certain depth in the powder layer. Above this onset of rapid decline, the distribution of the absorbance is quite homogenous. The reason for this region of even distribution is the effect of the absorption of scattered radiation in the powder. Absorption of laser radiation by the powder particles can be

formally split up into to different components: Direct absorption from attenuation by reflection or scattering of the un-scattered laser radiation $dA_{1st\,grade}$, and absorption due to already scattered radiation $dA_{scatter}$. For these ends it is necessary to break up the integral absorption functions $dA_{overall}$ in figure 3 into both respective components. The change of the three terms over powder layer depth (depth profiles) can be used to elucidate the individual effects of the components (figure 5, b).

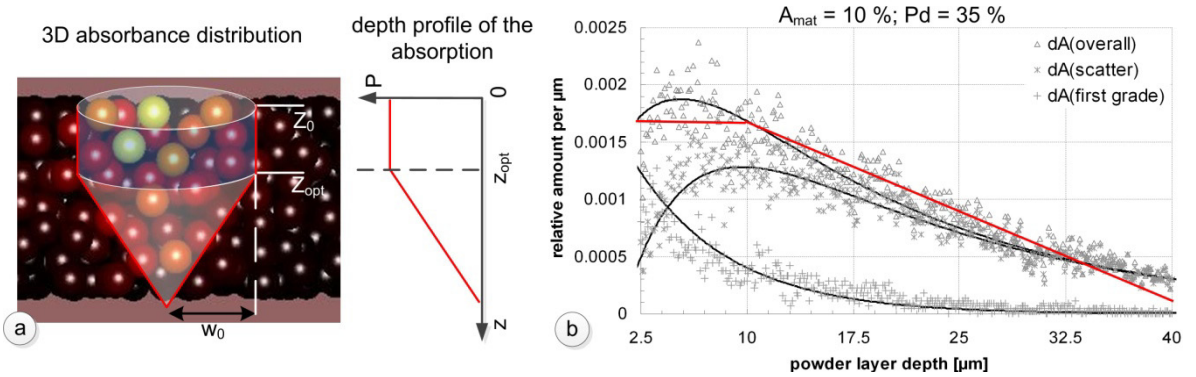

Fig. 5. For the presentation of the differential absorption functions $dA_{1st\,grade}$, and $dA_{scatter}$ the position and type of absorption for each individual scattering event was calculated and stored. The presented example is only valid for incident beams with Gaussian intensity profile. The plot of the data yields evidence for a powder volume between z_0 and z_{opt} with high and evenly distributed absorbance (b). The powder volume has approximately the shape of a cylinder with an adjacent down taper underneath (a).

The functions by which the two absorption components depend on the layer depth are different. There is a steady decline of 1st grade absorption $dA_{1st\,grade}$ at growing depth. Higher grade absorption $dA_{scatter}$, on the contrary, has a maximum that correlates with S_{for} according figure 5. The sum of both functions $dA_{overall}$ describes the differential absorption over the depth of the powder layer. Wang and Kruth, 2000, have pointed out this maximum, closely beneath the powder surface. It is decisive for the homogeneous absorbance distribution right beneath the layer surface, that the inclination of the higher grade absorption $dA_{scatter}$ makes up for the decline of 1st grade absorption $dA_{1st\,grade}$. This leads to a relatively even absorbance distribution within a limited depth range. In figure 5 this is highlighted in a streamlining manner by the red line. Beneath the horizon of maximum higher grade absorption $dA_{scatter}$ considerable decline of the overall absorbance $dA_{overall}$ occurs.

It is assumed that the maximum of higher grade absorption $dA_{scatter}$ coincides with the maximum of forward scattering S_{for} (figure 3) since this is the depth where maximum scattering is generated. As this maximum is always in the same depth range as the intersection between the respective curves of transmission T and integral absorption A, which is the depth of equivalence of those two terms, it is suggested, as a calculable approximation, that this point of equivalence of A and T shall be considered the depth of maximum grade absorption $dA_{scatter}$, and thus, consequently, the bottom level of the cylindrical powder volume with even and maximum absorbance distribution, as described in figure 5.

Therefore it is proposed that an important laser sinter parameter z_{opt}, the optimum powder depth or layer thickness shall be calculated by use of equations (1) and (3):

$$e^{\ln\left(1-\frac{3}{2}Pd\right)\cdot\frac{z_{opt}}{2r_P}} = \sqrt[3]{A_{mat}}\cdot\left(1-e^{\ln\left(1-\frac{3}{2}Pd\right)\cdot\sqrt[3]{A_{mat}}\cdot\frac{z_{opt}}{2r_P}}\right) \tag{4}$$

The solution of equation (4) can best be obtained via an iterative approach. Several solutions for various particle radii r_P and packing densities Pd are presented in figure 6.

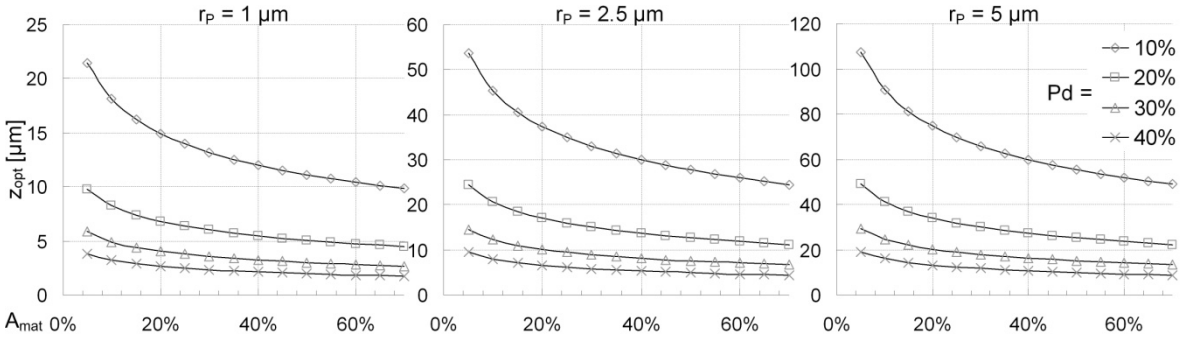

Fig. 6. Optimum powder layer thicknesses z_{opt} calculated according equation (4) with the potential of generating the maximum melt volume at the interface between powder and substrate body for various material specific absorption degrees A_{mat} and mono-disperse particle radii r_P.

8. Experimental corroboration

8.1. Single pulse sinter effect

Demonstrators for the zone of primary energy dissipation within irradiated powder can be produced only with high experimental effort. Shortly after the pulse, effects of concomitant secondary dissipation are superimposed. Furthermore, with higher laser beam intensities expulsion or eruption of material by plasma and other dynamic effects often occur before fusion of small melt phases to a noticeable sinter volume can evolve. For visualization purposes, therefore, powder has to be immobilized. This was solved by fixing the powder packing to a substrate with a conduction glue (to drain the heat form the glue) and condensing it by pressing a microscope slide on top. The resulting high powder density prevents the glue from being irradiated directly making sure that it is heated only after the fusion of the powder. When the glue gets heated subsequently it forms bubbles that shove or thrust those mainly porously fused powder entities out of their original positions in the packing. The cover slide saves those cross-linked units of particles from getting lost.

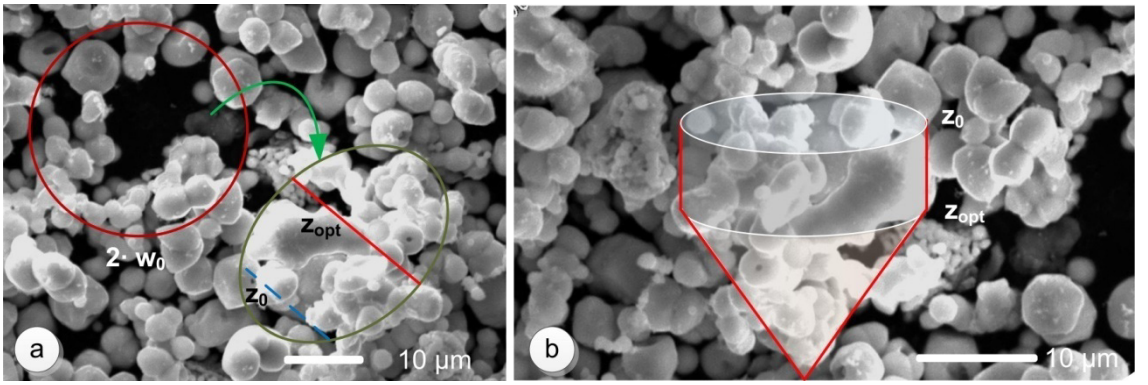

Fig. 7. Dense molybdenum powder packing that was charged with a single q-switched laser pulse. (a): Porously sintered ensemble of particles (green circle), that was dislocated from the original position (red circle) in the powder packing. Closer inspection reveals a decreasing occurrence of partially fused particles in the depth of the gap. (b): Comparison of the sintered unit with the assumed shape and dimension of the powder volume with high absorbance, according to fig. 5.

8.2. Sinter defects due to excessive thickness of powder layers

Figure 8 shows a series of probes that were generated with defined powder layer thickness excesses Δd. The excess was synthesized by omitting the sintering routine that was supposed to be performed after each powder coating for a definite number of cycles. In this manner the thickness of the powder layer was enhanced by definite amounts Δd above the optimum thickness that was 15 µm in the case of the employed powder. If the optimum layer thickness is exceeded by 8 µm there is still a chance that a sintered layer is sufficiently fused to the underlying sintered body (a). When the powder layer is thicker by 16 µm than the optimum height the layer is still fixed to the substrate, which is evident from its planeness, but only poorly since there is no sufficient heat conduction any more from the sintered layer to the bulk, detectable from the dark tarnish that the sintered layer has acquired (b). Almost no fusion at all can be observed, if the powder layer is by 32 µm deeper than the optimum thickness: The layer is warped and, of course, tarnished (c)

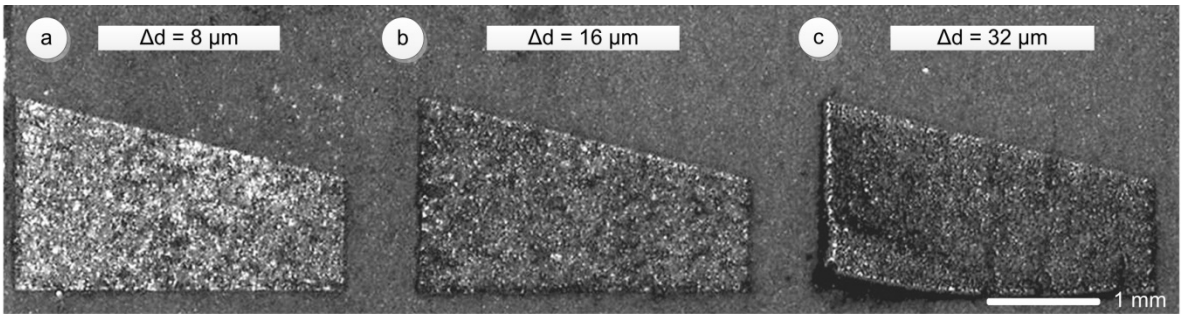

Fig. 8. Effects of thickness-excess Δd on the attachment of horizontally fused molybdenum powder onto the underlying bulk material. (a) (Δd = 8 µm): The sintered layer is still sufficiently fused to underlying bulk. (b) (Δd = 16 µm): A plane but tarnished sinter-layer is evidence for poor fusion to the bulk. (c) (Δd = 32 µm): A tarnished and warped sinter-layer means almost no fusion at all.

9. Summary and Outlook:

A ray tracing algorithm has been developed and applied to describe the primary power dissipation of a laser beam penetrating into a powder layer. “Primary dissipation” is the chosen term for deflection and absorption of coherent or scattered laser radiation. Because of the short pulse lengths implied in the regime of laser micro sintering this phase, to a certain degree, can be considered undisturbed by subsequent dissipation processes and its results are prerequisite for the onset of the sintering process. The characteristic quantities gained via the simulation of primary dissipation are the relative portions of the incident beam power, represented by transmission, forward and backward scattering, and absorption, as a function of the depth of penetration. The interdependence of these quantities and the shift of their balance along the depth are discussed for various sets of powder parameters. The position of maximum forward scattering can be approximated sufficiently by equating the analytically derived function for the transmitted power and the mathematical expression obtained by a fit of the backward scattering data. Further simulations that imply a laser beam with a Gaussian power distribution show that maximum concentration and an approximately even distribution of absorbance appears in a restricted powder volume between the surface of the powder layer and a level that resembles the position of maximum forward scattering. Thus, via this calculable lower depth limit a means for the determination of the optimum layer thickness for a powder with defined parameters has become available. It must be indicated, however, that the optimum sinter layer thickness can only be regarded as a starting condition of a laser sinter process especially for regimes employing q-switched laser pulses. Anticipation of the overall performance of laser sintering requires the consideration of further limitations that are imposed by the material behavior in the variety of processes that occur subsequent to the initial energy dissipation steps.

References

Gittard, S. D., Narayan, R. J., 2010. Laser direct writing of micro- and nano-scale medical devices, Expert Rev Med Devices. 2010 May; 7(3): pp. 343–356

Dobrzanski, L.A., Musztyfaga, M., Drygala, A., 2010. Selective laser sintering method of manufacturing front electrode of silicon solar cell, Journal of Achievements in Materials and Manufacturing Engineering 42, pp. 111–119

Tolochko, N. K., Khlopkov, Y. V., Mozzharov, S. E., Ignatiev, M. B., Laoui, T., Titov, V. I., 2000. Absorptance of powder materials suitable for laser sintering, Rapid Prototyping Journal, Volume 6, pp.155–161

Fischer, P., Karapatis, N., Romano, V., Glardon, R., Weber, H.P., 2002. A model for the interaction of near-infrared laser pulses with metal powders in selective laser sintering, Applied Physics A 74, pp. 467–474

Wang, X. C., Kruth, J. P., 2000. A simulation model for direct selective laser sintering of metal powders, in B. H. V. Topping (ed.), Computational Techniques for Materials, Composites and Composite Structures, pp. 57–71

Gusarov, A.V., Kruth, J. P., 2005. Modelling of radiation transfer in metallic powders at laser treatment, International Journal of Heat and Mass Transfer, Volume 48, pp. 3423–3434

Konrad, C., Zhang, Y., Shi, Y., 2007. Melting and resolidification of subcooled metal powder particle subjected to nanosecond laser heating, Int. Journal of Heat Mass Transfer, Volume 50, pp. 2236–2245